Geophys. J. Int. (1991) **105**, 561–571

Inferring the viscosity and the 3-D density structure of the mantle from geoid, topography and plate velocities

Yanick Ricard and Bai Wuming*
Département de Géologie, Ecole Normale Supérieure, 24 rue Lhomond, 75231 Paris Cedex 05, France

Accepted 1990 November 5. Received 1990 October 15; in original form 1990 March 27

SUMMARY

In a dynamic Earth, mantle mass heterogeneities induce gravity anomalies, surface velocities and surface topography. These lateral density heterogeneities can be estimated on the basis of seismic tomographic models. Recent papers have described a realistic circulation model that takes into account the observed plate geometry and is able to predict the rotation vectors of the present plates. The relationship between the surface observables and the heterogeneities is sensitive to the viscosity stratification of the mantle. Here we use this model, combined with a generalized least-squares method, in order to infer the viscosity profile of the Earth from the surface observations, and to get some new insight into the 3-D density structure of the mantle. The computed radial viscosity profile presents a continuous increase of more than two orders of magnitude. The asthenosphere has a viscosity close to 2×10^{20} Pa s. No sharp discontinuity is requested at the upper–lower mantle interface. The largest viscosity 7×10^{22} Pa s is reached in the middle of the lower mantle. At greater depth, approaching the core–mantle boundary, the viscosity decreases by one order of magnitude. The model suggests that the well-known degree-2 and order-2 anomaly in the transition zone of the upper mantle is merely the signature of the slabs. It also slightly increases the degree-2 and order-0 in the lower mantle and decreases it in the upper mantle. In other words the inversion requests a hotter lower mantle beneath the equator and a colder upper mantle at the same latitudes.

Key words: mantle density structure, mantle viscosity.

INTRODUCTION

The problem of deducing density structures from surface gravity data is known to lead to non-unique solutions. Of course with the assumption that all the mass anomalies lie at a prescribed depth or a prescribed interface like the Moho or the core–mantle boundary, different authors have performed such an inversion (e.g. Hide & Horai 1968). More complex methods have also been applied, minimizing the shear strain energy (Kaula 1963) or using the maximum entropy approach (Rubincam 1982). In all cases, the geophysical meaning of the assumptions leading to the inversion is, to the least, debatable. In what follows, we show that the combined inversion of the various geophysical data which are the topography, the geoid, the rotation poles and angular velocities of the plates reveals the long-wavelength structure of the Earth's mantle.

The presence of a given mass heterogeneity within the mantle not only modifies the gravity field but also induces a stress field which can be observed at the surface. This stress field affects the topography as well as the horizontal velocities. It is obvious that the topography, the geoid, and the velocity field are mostly sensitive to density variations located at different depths in the mantle. The topography is mainly related to the near-surface heterogeneities like the undulations of the Moho or the density increase of the cooling oceanic lithosphere. The plate motion has often been explained by means of two driving forces, slab pull and ridge push, counteracted by the mantle drag. These forces physically arise from the buoyancy differences between the average density of the mantle and the low density associated with ridges at depth or the high density associated with slabs. In some way, plate motion is revealing the structure of the top part of the mantle. In addition, the geoid, which is a very smooth integrator of the global mass distribution, allows us to put some constraints on the lower mantle density variations. Realistic relationships between the mass

* Permanent address: Laboratory of Geophysics, Academia Sinica, Beijing, China.

heterogeneities and their surface expressions, the topography, the geoid and plate motions, are therefore sampling the whole mantle.

THE FORWARD PROBLEM

The forward problem consists in computing the perturbations of the surface observables induced by a given mass located at a given depth. These computations have been carried out by different authors in the framework of purely viscous Newtonian Earth models with radial stratification. The answer has often been given in terms of Green functions. Such Green functions express the responses of an Earth model as the location depth of a source mass heterogeneity increases. In this formalism the heterogeneity has a vanishing thickness and is laterally described by a given harmonic degree. For any 3-D mass distribution, the solution can be found by a radial convolution and a horizontal summation of the spherical harmonics. Some authors (Richards & Hager 1984; Ricard, Fleitout & Froidevaux 1984) have mainly focused on the topography and gravity implications, whereas others have emphasized the relationships between mantle heterogeneities and plate motion (Forte & Peltier 1987).

This Green's function approach was used to constrain the viscosity stratification of the mantle (Hager 1984; Forte & Peltier 1987; Ricard, Vigny & Froidevaux 1989). However, this description suffers from a major drawback which was recognized long ago. Such models are unable to describe the lithospheric behaviour realistically, and they predict a surface motion which is very different from the observed one. The computed velocity field is said to be only 'poloidal' or 'without radial vorticity'. This means for example, that all the observed strike–slips between the plates cannot be explained. However for the real Earth the energy contained in the other velocity field component, called 'toroidal', is known to be close to the energy belonging to the poloidal field (Hager & O'Connell 1978).

In recent papers (Ricard & Vigny 1989; Vigny, Ricard & Froidevaux 1989; Bai *et al.* 1989) a new method has been proposed which can realistically predict the quasi-equipartition of energy between the two modes. The computation takes the real geometry of the existing plates into account. In this model, the knowledge of the poloidal, respectively toroidal, field and of the plate geometry imposes the toroidal, respectively poloidal, field. This assumption is right except for the toroidal field of degree 1. This field, which corresponds to a global rotation of the lithosphere is set by construction to zero in our model although it seems necessary for the description of the plate motions in the hotspots reference frame (Minster *et al.* 1974). The dynamics of a mantle overlaid by plates is found to be drastically different from what was predicted previously. As a consequence, the computed topography and gravity field are also affected by the presence of the plates.

The computational procedure is a generalization in 3-D spherical coordinates of an approach previously used in 2-D Cartesian geometry (Hager & O'Connell 1981). It is also akin to a more recent work on convection below rigid plates in 3-D parallelepipedic boxes (Gable, O'Connell & Travis 1988). The mathematical framework described in the papers previously quoted can be summarized as follow. First, the surface stress field generated by a 3-D mass distribution is computed, assuming a no-slip boundary condition at the surface of the Earth. Second, from the existing plate geometry, the surface stress field induced by a unit rotation of each plate around three orthogonal vectors is computed. Third, the rotation vectors are chosen in order to ensure that, on each plate, the stress field torque induced at step 1 is exactly balanced by the stress field torque related to plate motion. Fourth, with these rotation vectors and the internal mass anomalies the geoid and the topography are deduced.

In our model, the internal mass anomalies and the computed observables are expressed in terms of spherical harmonic coefficients. For a given viscosity profile and a given mass anomaly of degree l and order m, the response of the model is simply proportional to the amplitude of this mass, although this response can be of different degrees and orders. On the contrary, or a given mass distribution, the predictions of the model are linked to the viscosity profile by a non-linear relationship.

Mathematically, our approach is not entirely self-consistent. Indeed, a strict application of the concept of plate tectonics will lead to a velocity discontinuity at plate boundaries. This discontinuity produces a somewhat logarithmic singularity of the divergence of the stress field torque induced by forced plate motion, as a function of the degree l (Hager & O'Connell 1981). In other words, this means that we balance the internal stress field by an external one with an amplitude which increases with log l_{max}, the maximum degree used in the description of plate geometry.

We think however, that this behaviour cannot forbid to use this approach for two reasons. First, it is clear that the perfect rigidity of the plates is only a mathematical artefact. Using a maximum degree l_{max} for the computation only means that below the associated half-wavelength the plates are not rigid but perfectly plastic. Second, this singularity is rather smooth. Its effect is even less important if one considers the fact that the parameter we will invert for is the logarithm of the viscosity.

In this paper the maximum degree for the description of the plates is $l_{max} = 15$, corresponding to a half-wavelength of 1300 km. Had we assumed the plate to be rigid down to a half-wavelength of 100 km, we should have computed the stress field up to degree 195. Let us take the example of the Indian plate to illustrate the effect of truncation quantitatively. We compute the torque exerted by the velocity field of the observed plate motion (Minster & Jordan 1978) on this plate, for a mantle of uniform viscosity. The global velocity field has been truncated after a maximum degree l_{max} ranging from 1 to 15. Fig. 1 shows the dimensionless amplitude (left) and the longitude and latitude (right) of the resulting torque as a function of l_{max}. It is clear that if its amplitude has a singularity; its azimuth remains rather constant around 32°E and 63°N. The computed dimensionless torque is around 0.64 for $l_{max} = 15$. The effect of truncation is therefore to underestimate the torques necessary to drive the plates not their directions. After balancing the external stresses by the internal ones, only the average value of the mantle viscosity needed to move the plates will be affected by the truncation, not the relative viscosity profile. From Fig. 1, a rough extrapolation shows that the dimensionless amplitude of the torque

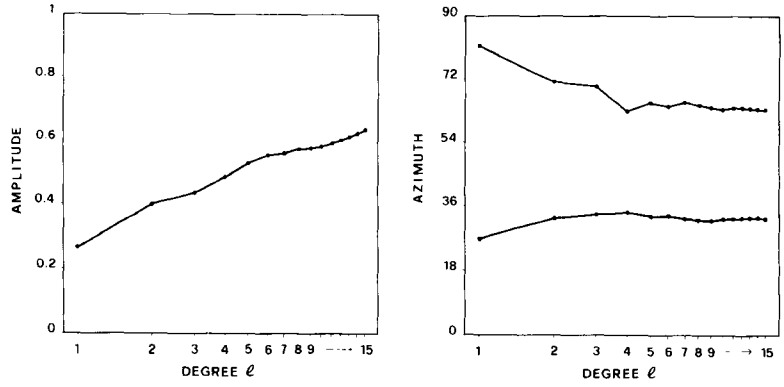

Figure 1. Torque applied on the Indian plate as a function of the truncation degree used for the description of plate motions and geometries. In the left graph, its dimensionless amplitude is depicted. In the right graph its longitude (lower branch °E) and latitude (upper branch °N) are shown. The direction of the torque remains rather constant whereas its amplitude increases with the logarithm of the truncation degree.

driving the Indian plate would have been around 1 if the computation had been carried out up to degree 195. This would have changed the external torque by a factor 1.6 at most, and decreased the averaged mantle viscosity requested to explain the observed plate velocities by the same amount. The viscosity profile on its logarithmic scale would have remained within the error bars of our inversion. A viscosity increase with depth would have strengthened this conclusion. In that case the shorter wavelengths which are only sampling the upper part of the mantle are sensitive to a lower viscosity than the long wavelengths. This decreases the short-wavelength components of the stress field. Thus, the torques would have been less affected by degree truncation.

The choice of a given degree truncation does not only affect the averaged mantle viscosity requested to explain the observed surface velocities but also changes the predicted geoid. On the one hand, the geoid component related to internal loads and computed with a no-slip boundary condition remains the same. On the other hand, the geoid component related to imposed surface velocities depends on the averaged mantle viscosity. Fortunately, this second component is weaker than the first one so that here again the problem of truncation does not seem to be crucial.

Another problem with our approach is related to the coupling between modes induced by the presence of plates. A mass of a given degree generates a flow also described by other degrees. As we only use a truncated series for the description of lateral mass anomalies, we cannot know what would be the effect of an additional mass with a smaller wavelength. However the dynamics of the real Earth with its characteristic plates is probably more closely described by our model than by the earlier radially stratified ones. In this paper, we will use mantle mass heterogeneities related to seismic tomography. Only the very large-scale features of the mantle (up to degree 6) are actually described. However we will show that even a restriction of our data set up to degree 5 will lead to comparable results.

An additional output of our model is the core–mantle dynamic topography. In the last few years different seismological studies have tried to map this topography. Unfortunately the available models are very different (Morelli & Dziewonski 1987; Creager & Jordan 1986; Doornbos & Hilton 1989) and the amplitudes they predict are unlikely to agree with physical constraints deduced from magneto-hydrodynamic studies (Hide 1989) or Earth rotation studies (Gwinn, Herring & Shapiro 1986). Furthermore, a study of the accuracy we can reach from the seismological data, in determining the core shape has shown that errors have an amplitude close to the detected signal (Gudmundsen 1989). It is also possible that the pattern observed by seismologists should not be related to a dynamic topography but rather to the sampling of D″ heterogeneities or to the presence of megaliths floating on the core. We have prudently chosen to ignore the important constraints that could be derived from these emerging additional data.

THE INVERSE PROBLEM

The forward problem relates the mantle heterogeneities to surface observations by means of a model computed on the basis of a radial viscosity distribution inside the Earth. The model is also slightly dependent upon the radial density of the Earth but we will assume this function to be exactly known. Our data $\mathbf{d}_0$ consists of the harmonic coefficients of the topography, the geoid and the poloidal surface field up to degree and order 6. The parameters $\mathbf{p}$ we want to invert for are, in principle, both the radial viscosity structure and the 3-D density structure. We will in fact perform two kinds of inversion separately, assuming first that the parameters are only the viscosities, and second that the densities are the unknowns to invert for. We define $\mathbf{g}$ as our model result such as $\mathbf{d} = \mathbf{g}(\mathbf{p})$ and $\mathbf{G}(\mathbf{p})$ is the matrix of the partial derivatives of $\mathbf{g}$ as a function of $\mathbf{p}$. This matrix is also computed by our program. The inverse problem is to derive $\mathbf{p}$ on the basis of the observed $\mathbf{d}_0$ and the theoretical models $\mathbf{g}(\mathbf{p})$ and $\mathbf{G}(\mathbf{p})$. Although it may be confusing, the same notations $\mathbf{g}(\mathbf{p})$ and $\mathbf{G}(\mathbf{p})$ are used for the two kinds of inversion. In the first case $\mathbf{g}(\mathbf{p})$ stands for the function relating the synthetic data to the viscosity assuming that the density heterogeneities are known. In the second case it relates the synthetic data to the density for a given viscosity profile. Similarly, $\mathbf{G}(\mathbf{p})$ stands for the partial derivatives of the synthetic data over the viscosity in the first case, and over the densities in the second one.

We have seen previously that the toroidal field can be deduced from the poloidal field, when the geometric

description of the plates is given. A perfect prediction of the poloidal field alone also leads to a perfect prediction of the toroidal field. Nevertheless, as a perfect fit will not be reached, inversions based on the toroidal field alone or on both fields would lead to different results. We have chosen to invert only the poloidal components for numerical convenience but we will check the high quality of our 'hidden' inversion of the toroidal components *a posteriori*.

Our inversion algorithm is the one given by Tarantola & Valette (1982) and consists in a fully probalistic approach. The basic aim of this inversion method is to minimize the following quantity:

$$\mathbf{I}(\mathbf{p}) = [\mathbf{d}_0 - \mathbf{g}(\mathbf{p})]^{\mathrm{T}} \mathbf{C}_{\mathbf{d}_0\mathbf{d}_0}^{-1} [\mathbf{d}_0 - \mathbf{g}(\mathbf{p})] + (\mathbf{p} - \mathbf{p}_0)^{\mathrm{T}} \mathbf{C}_{\mathbf{p}_0\mathbf{p}_0}^{-1} (\mathbf{p} - \mathbf{p}_0). \quad (1)$$

This formulation allows for slightly non-linear problems and has the advantage of explicitly including the *a priori* knowledge on the parameters. This knowledge enters both in the *a priori* guess for the parameters $\mathbf{p}_0$ and in their covariance matric $\mathbf{C}_{\mathbf{p}_0\mathbf{p}_0}$. This matrix contains on its diagonal the squares of the uncertainties on the parameters and on its off-diagonal elements the trade-off between them, related to the required smoothness of the results. This formalism also requires a data covariance matrix $\mathbf{C}_{\mathbf{d}_0\mathbf{d}_0}$ which allows the non-dimensionalization of the data vector. In addition, for the linear case, this method easily gives the resolution and the *a posteriori* covariance matrices describing the uncertainties and trade-offs.

The data vector $\mathbf{d}_0$ can be divided into three parts. One describes the topography, the second the geoid, and the third the poloidal velocity. The amplitude spectra of the three components decrease sharply with the degree l. The first two components have the dimension of length, the last one of velocity. The Earth's topography, corrected from the thickness of the oceans and filtered out for degrees larger than 6 has a peak-to-peak amplitude around 6000 m, the geoid around 200 m and the poloidal velocity field around 10 cm yr^{-1}. We chose a purely diagonal data covariance matrix and we want to fit the data vector with uncertainties corresponding to the root squares of the diagonal elements. We admit an uncertainty of 1000 m on the topography, 10 m on the geoid and 1 cm yr^{-1} for the velocity. These coefficients show that our inversion is weighted in such a way that the resulting model mainly tries to fit the geoid (10 m over 200 m), less the velocity (1 cm yr^{-1} over 10 cm yr^{-1}) and least the topography (1000 m over 6000 m). Because the elements of the covariance matrix are independent of the degree, our inversion will try to model the long-wavelength features more precisely than those of short wavelength.

The constraints provided by the topography needs some comments. The topography is, of course, mainly due to the existence of the Moho. Our model predicts a dynamic topography which also includes the isostatic compensation of shallow sources. However, such a compensation mechanism will not constrain the viscosity profile of the mantle. Two different approaches could have been used to include the topography in our inversion scheme. First we could have considered only the topography related to mantle mass heterogeneities. This could be obtained by peeling the observed topography from the effects of the Moho undulations. The remaining topography includes the cooling of the oceanic lithosphere. It may also include other features which are very difficult to observe, such as an anomalous oceanic topography of degree 2 and amplitude around 400 m, highly correlated with the geoid (Cazenave, Souriau & Dominh 1989). This feature is possibly related to lower mantle convection but may be only an artefact due to incomplete data analysis (Colin & Fleitout 1990). Second, we can take into account the whole topography corrected for the ocean water density, including in our *a priori* density structure the shape of the Moho. For simplicity we chose this last solution. Our Moho description (Dziewonski 1984) explains, whatever the mantle viscosity may be, 50 per cent of the Earth's topography. This means that the constraints brought by the topography are very weak since we want to explain a remaining topography of about 50 per cent of 6000 m with uncertainties of 1000 m.

INVERSION OF THE RADIAL VISCOSITY

As a first step will assume the mantle mass heterogeneities to be perfectly known and we will invert for the viscosity structure. We assume the mantle heterogeneities to be proportional to the seismic velocities deduced from the tomographic models of Woodhouse & Dziewonski (1984) for the upper mantle and Dziewonski (1984) for the lower mantle. The proportionality constants $dV_S/d\rho$ and $dV_P/d\rho$ have been chosen equal to 6 km s^{-1}g^{-1}cm^3 and to 4 km s^{-1}g^{-1}cm^3. These derivatives are close to experimental results obtained by changing the temperatures of rock samples. We have also tested other values and a possible depth increase of these coefficients (Hong & Yuen 1989) related to a strong decrease in the thermal expansion coefficient with depth (Chopelas & Bohler 1989), but our results did not differ substantially.

The geoid and the topography are only related to relative variations of the viscosity whereas the velocity depends upon the absolute values. The absolute viscosity of the Earth can also exhibit very large variations, say from 10^{19} to 10^{23} Pa s. As a consequence, we have chosen our parameters to be first, the logarithm of the averaged mantle viscosity $p(1) = \log_{10}\eta_0$, and then, the logarithms of the ratio of the viscosity at the radii r_i, over the averaged viscosity $p(i) = \log_{10}[\eta(r_i)/\eta_0]$. The number of radii r_i taken into consideration is 15. We also need to define the *a priori* viscosity profile and the *a priori* parameter covariance matrix. We have built this matrix with the following form:

$$\mathbf{C}_{\mathbf{p}_0\mathbf{p}_0}(i,j) = \begin{cases} \sigma_1^2 \delta_{ij}, & \text{if } i = 1 \text{ or } j = 1, \\ \sigma_2^2 \exp\left(-\dfrac{(r_i - r_j)^2}{2\Delta^2}\right), & \text{if } i \neq 1 \text{ and } j \neq 1. \end{cases} \quad (2)$$

We have chosen an uncertainty σ_1 equal to 2 and σ_2 equal to 0.75. This means that we suggest an uncertainty of two orders of magnitude on the *a priori* average viscosity which is taken equal to 10^{21} Pa s [$p_0(1) = 21$], and an uncertainty less than one order of magnitude on the relative viscosity profile [$p_0(i) = 0$, for $i = 2$ to 16]. The correlation length Δ is 400 km in both the upper and lower mantle.

Tarantola & Valette have proposed different formulations of their algorithm, depending on the relative sizes of the data and the parameter vectors. In our case, a purely

overdetermined problem, we compute the solution iteratively, starting from $\mathbf{p}_0$ and obtaining sucessively $\mathbf{p}_k$, $\mathbf{p}_{k+1}$. From the solution at the step k we compute $\Delta\mathbf{p}$ given by

$$\Delta\mathbf{p} = (\mathbf{G}_k^T \mathbf{C}_{\mathbf{d}_0\mathbf{d}_0}^{-1} \mathbf{G}_k + \mathbf{C}_{\mathbf{p}_0\mathbf{p}_0}^{-1})^{-1} \times \{\mathbf{G}_k^T \mathbf{C}_{\mathbf{d}_0\mathbf{d}_0}^{-1} [\mathbf{d}_0 - \mathbf{g}(\mathbf{p}_k)] + \mathbf{C}_{\mathbf{p}_0\mathbf{p}_0}^{-1} (\mathbf{p}_0 - \mathbf{p}_k)\}. \quad (3a)$$

Then we deduce the solution at the step $k + 1$:

$$\mathbf{p}_{k+1} = \mathbf{p}_k + \alpha\Delta\mathbf{p} \quad (3b)$$

where $\mathbf{I}(\mathbf{p}_{k+1})$ given by equation (1) is minimum under the assumption $\alpha \in [0, 2]$. We add this minimization step to the Tarantola & Valette procedure where α is 1. A minimum has always been found in the direction proposed by equation (3) with $\alpha \in [0, 2]$. The stable $\mathbf{p}$ model is reached after three or four iterations. Without the minimization step, however, the convergence is generally slower, and sometimes a stable but oscillating behaviour is obtained.

The resolution and trade-off of the solution can be discussed in terms of resolution kernels (Backus & Gilbert 1970). The computed parameters are in fact the average of the real parameters weighted by the resolution matrix. For our algorithm, but in the linear case, the resolution matrix takes the form (Montagner & Jobert 1981)

$$\mathbf{R} = (\mathbf{G}^T \mathbf{C}_{\mathbf{d}_0\mathbf{d}_0}^{-1} \mathbf{G} + \mathbf{C}_{\mathbf{p}_0\mathbf{p}_0}^{-1})^{-1} \mathbf{G}^T \mathbf{C}_{\mathbf{d}_0\mathbf{d}_0}^{-1} \mathbf{G}. \quad (4)$$

A satisfactory inversion leads to a resolution matrix close to identity. In the non-linear case no analytical expression can be found. However, we use equation (4), where $\mathbf{G}$ is computed with the parameters of the solution as a qualitative but reliable estimation of the real resolution matrix.

We also use the linear expression of the *a posteriori* covariance matrix as a good estimator of the uncertainties of the model:

$$\mathbf{C}_{\mathbf{pp}} = (\mathbf{I} - \mathbf{R})\mathbf{C}_{\mathbf{p}_0\mathbf{p}_0}. \quad (5)$$

In this equation, $\mathbf{I}$ is the identity matrix.

Figure 2 shows the result of the inversion. The dashed line depicts the *a priori* viscosity taken here as uniform, and the thick line the inverted profile. One should remember that the mantle is overlaid by a rigid lithosphere broken into 11 main plates. The thin lines are the uncertainties deduced from the *a posteriori* covariance matrix. The solution does not exhibit a very sharp viscosity increase near the upper–lower mantle interface, but rather a regular slope over about two orders of magnitude. The largest viscosity is reached in the middle of the lower mantle. A strong viscosity decrease also appears near the core–mantle boundary. The averaged mantle viscosity related to $p(1)$ is $\eta_0 = 2 \times 10^{21}$ Pa s. This value is in good agreement with the averaged mantle viscosity deduced from post-glacial rebound.

The turning point in the depth derivative of the viscosity profile has important implications for the pressure and temperature dependence of the rheology and for convection studies. The usual viscosity laws are decreasing with temperature and increasing with pressure. However we cannot easily derive the temperature dependence directly from the depth variation of the viscosity, as the temperature profile is itself the result of the convective behaviour. When the temperature gradient is adiabatic, the pressure effect

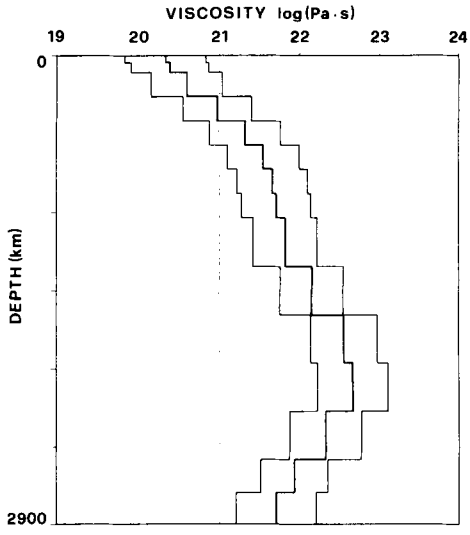

Figure 2. Viscosity of the mantle as a function of depth deduced from our inversion (thick line). 15 layers have been considered for the inversion. The uncertainties deduced from the diagonal of the *a posteriori* covariance matrix are also depicted (thin lines). Our *a priori* profile is a constant viscosity model ($\eta = 10^{21}$ Pa s) shown by the dashed line. The lithosphere on the top consists of the 11 main plates, described as rigid bodies separated by infinitely weak boundaries.

dominates and the viscosity increases with depth. The existence of a negative slope in the bottom of the lower mantle indicates that the temperature variation overcomes the pressure effect. This observation may reveal the presence of a temperature gradient larger than the adiabatic one.

This profile is not greatly changed when a different *a priori* viscosity is chosen. The solution is also quite independent of the absolute value of the starting average viscosity $p_0(1)$. Fig. 3 (full line) depicts the results obtained when a viscosity increase by a factor 10 is imposed in the *a priori* model at the upper–lower mantle interface. The viscosities on both sides of this interface are also supposed to be uncorrelated. Within their uncertainties, the two profiles of Figs 2 and 3 are the same. When a larger viscosity increase is proposed, the inversion tends to damp it. One can also use an *a priori* solution $\mathbf{p}_0$ equal to the *a posteriori* solution $\mathbf{p}$ of a previous inversion. This, of course, leads to an artificial reduction of the misfit expressed by the equation (1). However, the improvement is small, and the final profile stays very close to that depicted in Fig. 2 or 3. The general shape and absolute values of our viscosity profile are not drastically affected when we use different sets of parameters for the *a priori* covariance matrix or for the proportionality factors between seismic velocities and density.

To verify that our model is not too dependent upon the truncation degree used in the description of internal mass anomalies, we performed another inversion taking only the five first degrees for the internal masses. The derived plate motions are always expressed up to degree 15. The inverted profile is also plotted in Fig. 3 (dashed line). Despite a somewhat larger amplitude the general shape of the profile remains the same.

The topography has a low weight in our inversion, but to confirm that we are not mapping errors in the crustal

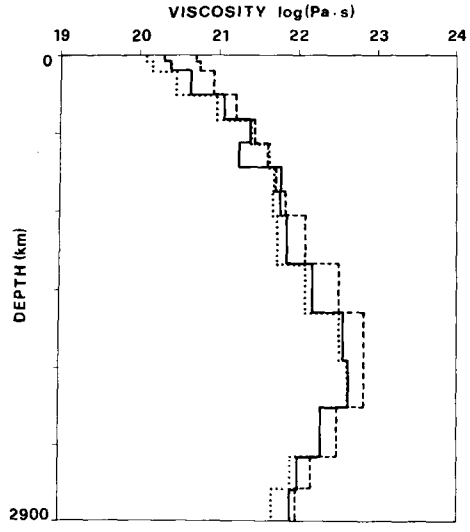

Figure 3. Three viscosity profiles deduced from different assumptions. The full line corresponds to an inversion obtained with an *a priori* uniform viscosity. One (dashed line) depicts the results when only the five first degrees of the tomography are taken into account, *priori* unifrom viscosity. One (dashed line) depicts the results when only the five first degrees of the tomography are taken into account, the other (dotted line) when the topography data are not considered. The three curves lie within the uncertainties of the profile plotted in Fig. 2.

thickness into a spurious viscosity distribution, we invert our data without taking into account the Moho undulations and without fitting the topography. The resulting profile (Fig. 3, dotted line) does not differ much from the other ones.

In a previous paper (Ricard *et al.* 1989), we have shown that a good fit can also be attained with a viscosity profile having a hard garnet layer in the transition zone above the upper–lower mantle boundary (Karato 1989). This result was obtained assuming that upper mantle seismic anomalies are of chemical origin and using in this layer a density distribution mapping the slabs. As satisfactory predictions have been obtained in the present study with the simplest assumption of thermally induced upper mantle anomalies, we did not try our inversion starting from a viscosity profile having a hard garnet layer and using density anomalies related to slabs in the first 700 km depth. However, we performed another inversion with the density anomalies related to the tomography but assuming an *a priori* viscosity profile with a stiff layer in the bottom of the upper mantle. The viscosity of this layer was supposed to be uncorrelated with others. We again derived a profile quite close to those depicted in Figs 2 and 3.

The resolution matrix of our inversion is depicted in Fig. 4. It is computed using the viscosities depicted in Fig. 2, deduced from an *a priori* uniform profile. Nevertheless, the resolution matrix is basically the same when other *a priori* parameters are chosen. This resolution is not equal to the identity matrix as it would have been for a perfect inversion, but the maximum is always reached on the diagonal. Some leakage appears between the determined mantle viscosities in the top and bottom of the lower mantle. However we think that this resolution matrix shows that our inversion is indeed meaningful.

Figure 5 depicts the fit to the data our inversion reaches. We have computed both the correlation coefficients (bottom row) and the mean percentages of variance which are explained (top row) for the different degrees. The four columns successively show the results for the topography, the geoid, the poloidal and the toroidal components. As we noted before, the real inversion of this last component has not been carried out but is naturally achieved by our formalism. All but one of the correlation coefficients are

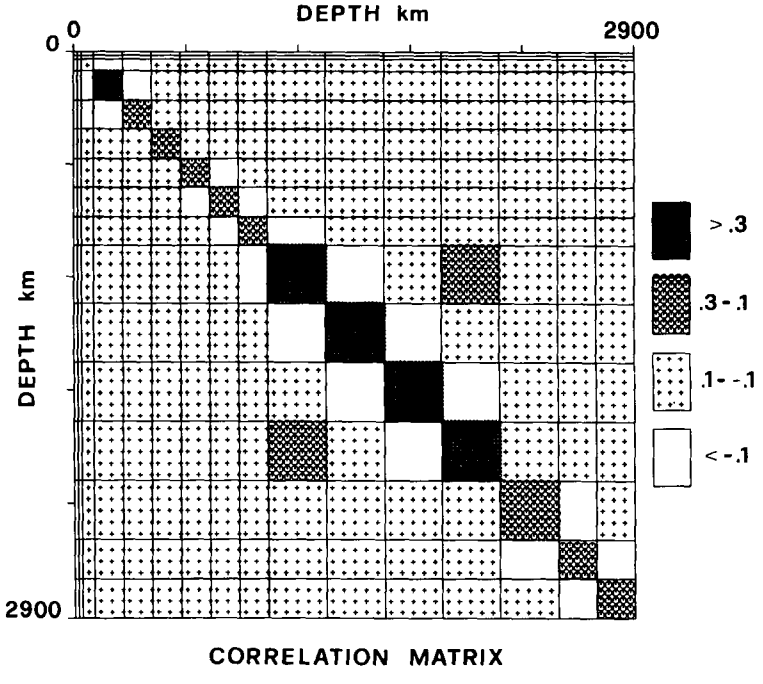

Figure 4. Resolution matrix of the inversion leading to the viscosity profile of Fig. 1. The grey scale shows the values larger than 0.3 (darkest), between 0.3 and 0.1, and between 0.1 and −0.1 (lighter). The matrix elements in white are between −0.1 and the minimum found to be −0.2.

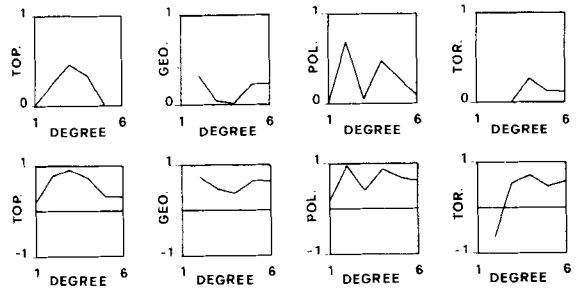

Figure 5. Correlation coefficients (bottom row) and percentages of variance reduction of the data (upper row) as a function of the degree l. From left to right are depicted the results for the topography, the geoid, the poloidal components, and the toroidal components of surface velocities. A perfect prediction would lead to a correlation coefficient equal to 1 and 1 = 100 per cent of explanation. A correlation equal to 1 is associated with an explanation percentage of 100 per cent only when the amplitudes of synthetics and data are equal.

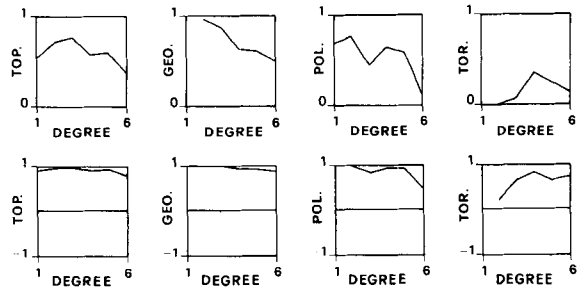

Figure 6. Correlation coefficients (bottom row) and percentage of variance reduction (upper row) as a function of the degree l, after the inversion for the density structure. As in Fig. 4, from left to right are depicted the results for the topography, the geoid, the poloidal components, and the toroidal components. By comparison with the previous figure, we note the much higher quality of the fit.

positive and most of them are meaningful. However, when the six degrees are taken together with their relative amplitudes, our model only accounts for about 35 per cent of the topography, 25 per cent of the geoid, 10 per cent of the poloidal field and a few per cent of the toroidal one. These last two fields are related to the surface horizontal divergence and radial vorticity, two quantities which are perhaps more easily understood by our physical intuition. The spectra of the horizontal divergence and radial vorticity are obtained by multiplying the spectra of the poloidal and toroidal fields by $l(l+1)$. The observations show that they reach their maxima for $l = 4$ and $l = 5$, the degrees where the correlations are found to be significant. One can thus be more optimistic about the quality of our fit which explains 30 per cent of the horizontal divergence and 15 per cent of the radial vorticity.

More satisfactory predictions of the geoid from mantle anomalies have been derived using the same approach but different density sources (Richards & Hager 1988). The discrepancy only occurs from the use of different tomographic models. These authors are using the results of Clayton & Comer (1983), eventually completed in the upper mantle by the model of Tanimoto (1986). They also introduced an *ad hoc* density distribution mapping the slabs (Richards & Hager 1988). However, the quality of our fit is comparable with what has been obtained elsewhere with the tomographic models we use (Forte & Peltier 1987). Furthermore the common inversion of geoid, plate motion and topography somewhat degrades the fit which might be reached from the separate inversions of the three data sets. In our inversion we only try to start from the simplest and most objective data set.

INVERSION OF THE 3-D DENSITY STRUCTURE

As a second step we try to solve the more presumptuous problem which consists of finding the internal mass heterogeneities which are requested by our model to explain the surface observations. In this case the viscosity profile is supposed to be known and we will take the solution found in the previous section. The parameters are the density heterogeneities at 15 different depths up to degree and order 6. Of course, the number of unknowns is now much larger than the number of data. The inversion is made possible by the *a priori* knowledge we assume for the definition of the *a priori* density model and its associated covariance matrix. We chose this model to be the one used previously; that means a density structure simply proportional to the seismic tomography. The uncertainties and correlation lengths needed in order to build the covariance matrix have been chosen in the following way. In the mantle, we take the same correlation length as in our previous inversion $\Delta = 400$ km. We assume no correlation between our first layer, describing the crustal heterogeneities, and the mantle. The uncertainties in the density structure at a given depth are proportional to the square root of l and amount to 50 per cent of the variance in the *a priori* density structure at the same depth and for the degree $l = 1$. The absolute uncertainties for degree 6 are thus, supposed to be 2.5 ($=\sqrt{6}$) larger than for degree 1.

Following Tarantola & Valette (1982) the solution of this underdetermined problem reads

$$\mathbf{p} = \mathbf{p}_0 + \mathbf{C}_{\mathbf{p}_0\mathbf{p}_0}\mathbf{G}^T(\mathbf{C}_{\mathbf{d}_0\mathbf{d}_0} + \mathbf{G}\mathbf{C}_{\mathbf{p}_0\mathbf{p}_0}\mathbf{G}^T)^{-1}(\mathbf{d}_0 - \mathbf{G}\mathbf{p}_0). \quad (7)$$

In that case, the relationship between parameters and density is linear and the solution is reached without iterations. We will not discuss the *a posteriori* covariance matrix as its interpretation is too complex, involving the

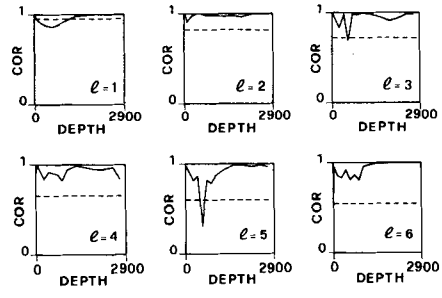

Figure 7. Correlation coefficients as a function of depth between the tomographic data and the inverted 3-D density structure. The different degrees from 1 to 3 (top row) and 4 to 6 (bottom row) are displayed from left to right. The 95 per cent confidence levels are also depicted (dashed lines).

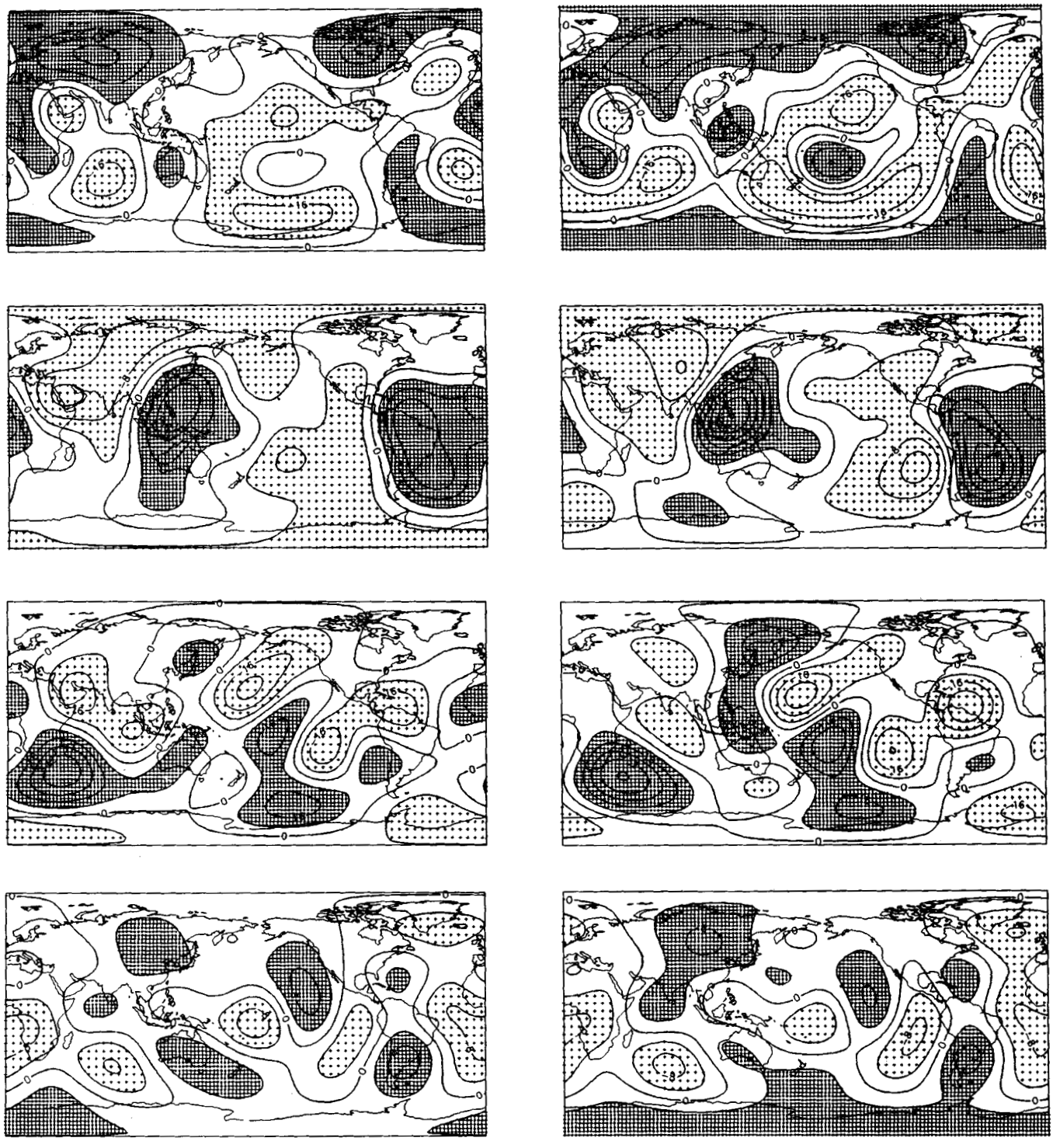

Figure 8. Comparison between the *a priori* density anomalies at the depths of 250, 550, 700 and 2200 km which are assumed to be proportional to the seismic tomography models (left column) and the density pattern at the same depths deduced from our inversion (right column). The high-density anomalies are shown in dark shading, the low-density anomalies in light shading. The scales are the same in a given row. The level lines are 8 kg m^{-3} apart in the first and third rows, 4 kg m^{-3} apart in the second and fourth rows. The correlations between two corresponding maps are obvious. In the upper mantle the results of our inversion are more clearly underlining the surface tectonic provinces like ridges, old cratons or slabs.

cross-correlation products of mass heterogeneities at a given depth and given degree and order with other masses at different depths, degrees and orders.

Figure 6 shows the fit between the data $\mathbf{d}_0$ and the synthetics **Gp** computed from the 3-D density structure obtained after the inversion. Comparing with Fig. 5, which depicted the fit deduced from the tomographic models $\mathbf{Gp}_0$, we see that the correlations (bottom row) and percentage of data which are explained (top row) have been significantly increased for all degrees. Even for the toroidal part which is not explicitly included in our inversion the fit is much better. Due to the rapidly decreasing spectra of both the geoid and the plate velocities (Hager & O'Connell 1978), the inversion procedure has preferentially improved the prediction of the lowest degrees. Of course, playing with the *a priori* covariance matrix one can obtain better fits as the inverted density structure goes away from the starting one proportional to tomography.

Figure 7 depicts the correlations between the tomography and the inverted density structure as a function of depth and for the different degrees. We also plot with dashed lines the confidence levels at 95 per cent. The correlations for all degrees between the starting and the final models are very high. The inversion hardly modifies the degree two of our starting model which appears to be the best resolved degree throughout the mantle. In the upper mantle, the even degrees 2, 4, and 6 remain more stable than the odd degrees 1, 3, and 5. This behaviour is consistent with the fact that the upper mantle tomography has much better resolution for even degrees than for odd degrees (Woodhouse & Dziewonski 1984).

Previous studies have shown that the tomographic models used here cannot predict the correct polar flattening (Ricard *et al.* 1989). The inverted density leads by construction, to a better fit. This is obtained by increasing the term of degree 2 order 0 in the lower mantle and decreasing it in the upper one. This means that the algorithm proposes a somewhat stronger zonal structure that was suggested by tomography. The lower mantle could be less dense near equatorial latitudes than polar ones and this structure should be reversed in the upper mantle. Of course, because of the coupling between modes due to the plates, other degrees and orders of the internal mass distribution also contribute to the geoid of degree 2 and order 0.

We have chosen to depict the resulting mass distributions at four different depths. Fig. 8 shows the inverted density at 250, 550, 700 and 2200 km depths (right column) compared with the seismic tomography scaled in density for the same depths (left column). At shallow depths, our results appear to have a better correlation with the tectonic features than the tomographic results. In the first row, the low-density regions deduced from our inversion follow the ridges everywhere with a lower amplitude under the North Atlantic. The Antarctic craton is also associated with a dense root. The most interesting remark about the results of this inversion comes perhaps from the second and third rows of Fig. 8. Although at 550 km depth the degree 2 of the two maps is quite similar, our inversion underlines more clearly the existence of the slabs around the Pacific. Even at 700 km, one can follow this slab distribution in the western part of the Pacific ocean. This suggests that the well-known degree 2 in the transition zone could be only the shadow of the slabs, their higher degrees being missed by the tomography. In the lower mantle (bottom row), the inverted density remains close to the *a priori* one, although its zonal structure has been somewhat enhanced. At this depth, one notes the strong anticorrelation between the density anomalies and the surface geoid.

We also performed our inversion without taking into aaccount the density anomalies associated with the Moho in our *a priori* density structure and without fitting the topography. The inverted density pattern remains unchanged except in the first layers for depths smaller than 100 km. This is a strong indication that, according to our choice of the density covariance matrix, the inversion does not lead to the spurious mapping of crustal anomalies into the mantle.

DISCUSSION

The radial viscosity profile of the Earth is a very debatable subject. Different geophysical phenomena are related to this quantity, but they are not sampling this parameter during the same characteristic times. The post-glacial rebound (e.g. Peltier & Andrews 1976; Wu & Peltier 1983) and the related effects such as the change in the polar flattening or the secular polar wander (Sabadini & Peltier 1981) have characteristic time constants of about 10 000 yr. The importance of transient rheology cannot be precisely quantified and could hide the long-term mantle behaviour. The modelling of the geoid, topography and plate motion requests time constants of millions of years. The long-term true polar wander deduced from palaeomagnetism (Sabadini & Yuen 1989) also occurs on the same temporal scale.

The post-glacial readjustment can be explained by a rather uniform mantle where the viscosity jump at the upper–lower mantle interface is less than one order of magnitude (Mitrovica & Peltier 1989). However some authors have performed a satisfactory fit with an asthenospheric upper mantle channel on top of a rigid lower mantle (Officer *et al.* 1988). Less extreme stratification has also been proposed by Nakada & Lambeck (1989). Their model is roughly the same as the one we propose with an upper mantle viscosity of about 10^{20}–10^{21} Pa s and a viscosity increase by a factor 100 in the lower mantle. It thus seems that post-glacial rebound is mainly sensitive to upper mantle viscosity and that the upper mantle viscosity it requires agrees with ours.

The studies of observed actual polar wander have also favoured a rather uniform mantle structure. However depending only on phenomenon of degree 2, their resolution of the Earth's stratification remains poor. Furthermore, the data can generally be fitted by two different profiles: one with a uniform mantle, and another with a strong viscosity increase (Yuen *et al.* 1986). This last solution has sometimes only been discarded in order to satisfy some previous post-glacial rebound studies.

The necessity of an important stratification of the mantle, clained by geochemists (e.g. Allègre 1982), has also been advocated by other workers following the same approach as ours, but with simpler inversion procedures (Hager *et al.* 1985). The same viscosity profile also arises from the study of long-term polar wander (Sabadini & Yuen 1989; Ricard & Sabadini 1990). One can perhaps be more confident in the

results of this set of studies dealing with very slow processes than on the extrapolation for million years of studies of phenomena arising in a few thousand years.

The viscosity model we have used has a radial symmetry but allows for the individual plate displacements. We are aware that our approach introduces stress singularities at plate boundary but we think that it catches the basic physics of the mantle circulation. The temperature differences that induce density variations also lead to lateral viscosity variations. This effect would modify our results by an amount which does not seem to be of prime importance (Richards & Hager 1989). The viscosity profile we propose, is basically characterized by three points. It exhibits a weak asthenosphere with low viscosity, 2×10^{20} Pa s, which allows for the plate motion. No viscosity jump is required at the upper–lower mantle interface. After having reached a maximum, 7×10^{22} Pa s, the viscosity decreases in the bottom third of the lower mantle. We hope that these results can help constrain the thermal structure of the lower mantle and the temperature and pressure dependence of the viscosity.

The mass distribution deduced from our inversion must be taken with caution. First, the problem is largely underdetermined, and second, the answer is biased by the first inversion step. Our viscosity profile indeed favours mass heterogeneities close to those of the tomographic models used as input in our first inversion. However, the density structure derived from our inversion has many simple and realistic characteristics. The heterogeneities close to the surface are even more correlated with the surface tectonics than what is suggested by the tomography. The slabs are the major anomalies within the transition zone. We may hope that in future the improvement of the tomographic models and the addition of new data, such as the core–mantle topography will allow for a more meaningful inversion. Moreover, this kind of geophysical modelling joined with seismic tomography shows a possible way to distinguish between density and elastic property variations.

ACKNOWLEDGMENTS

This work was partly supported by the Institut National des Sciences de l'Univers (INSU-DBT 'Dynamique Globale' contribution no. 230).

REFERENCES

Allègre, C. J., 1982. Chemical geodynamics, *Tectonophysics*, **81**, 109–113.

Bai, W., Vigny, C., Ricard, Y. & Froidevaux, C., 1991. On the origin of deviatoric stresses in the lithosphere, *J. geophys. Res.*, in press.

Backus, G. & Gilbert, F., 1970. Uniqueness in the inversion of inaccurate gross Earth data, *Phil. Trans. R. Soc. Lond.*, **266**, 123–192.

Cazenave, A., Souriau, A. & Dominh, K., 1989. Earth surface topography: global coupling with hotspots, geoid and mantle heterogeneities, *Nature*, **340**, 54–57.

Chopelas, A. & Bohler, R., 1989. Thermal expansion measurements at very high pressure, systematics and a case for a chemically homogeneous mantle, *Geophys. Res. Lett.*, **16**, 1347–1350.

Clayton, R. W. & Comer, R. P., 1983. A tomographic analysis of mantle heterogeneities from body wave travel times, *EOS, Trans. Am. geophys. Un.*, **64**, 776.

Colin, P. & Fleitout, L., 1990. Topography of the ocean floor: thermal evolution of the lithosphere and interaction of deep mantle heterogeneities with the lithosphere, *Geophys. Res. Lett.*, **17**, 1961–1964.

Creager, K. C. & Jordan, T. H., 1986. Aspherical structure of the core–mantle boundary from PKP travel time, *Geophys. Res. Lett.*, **13**, 1497–1500.

Doornbos, D. J. & Hilton, T., 1989. Models of the core–mantle boundary and the travel times of internally reflected core phases, EGS, *Annales Geophysicae*, special issue, 44.

Dziewonski, A. M., 1984. Mapping the lower mantle: determination of lateral heterogeneity in P velocity up to degree and order 6, *J. geophys. Res.*, **89**, 5929–5952.

Forte, A. M. & Peltier, W. R., 1987. Plate tectonics and aspheroidal Earth structure: the importance of poloidal–toroidal coupling, *J. geophys. Res.*, **92**, 3645–3679.

Gable, C. W., O'Connell, R. J. & Travis, B. J., 1988. Plate motion in models of 3-D convection with layered viscosity: implications for mantle flow, *EOS, Trans. Am. geophys. Un.*, **69**, 1414.

Gudmundsson, O., 1989. Some problems in global tomography: modelling the core–mantle boundary and statistical analysis of travel-time data, *PhD thesis*, Caltech, Pasadena, CA.

Gwinn, C. R., Herring, T. A. & Shapiro, I. I., 1986. Geodesy by radio interferometry, studies of the forced nutations of the Earth, 2, Interpretation, *J. geophys. Res.*, **91**, 4755–4765.

Hager, B. H., 1984. Subducted slabs and the geoid: constraints on mantle rheology and flow, *J. geophys. Res.*, **89**, 6003–6016.

Hager, B. H. & O'Connell, R. J., 1978. Kinematic models of large-scale flow in the Earth's mantle, *J. geophys. Res.*, **84**, 1031–1048.

Hager, B. H. & O'Connell, R. J., 1981. A simple global model of plate dynamics and mantle convection, *J. geophys. Res.*, **86**, 4843–4867.

Hager, B. H., Clayton, R. W., Richards, M. A., Comer, R. P. & Dziewonski, A. M., 1985. Lower mantle heterogeneity, dynamic topography, and the geoid, *Nature*, **313**, 541–545.

Hide, R., 1989. Fluctuations in the Earth's rotation and the topography of the core–mantle interface, EGS, *Annales Geophysicae*, special issue, 43.

Hide, R. & Horai, K. I., 1968. On the topography of the core–mantle interface, *Phys. Earth planet. Inter.*, **1**, 305–308.

Hong, H.-J. & Yuen, D. A., 1989. Dynamical influences on topography and geoid from recent high-pressure experiments: variations of $d \ln V / d \ln p$ with depth, *EOS, Trans. Am. geophys. Un.*, **70**, 1359.

Karato, S., 1989. Plasticity-crystal structure systematics in dense oxides and its implications for the creep strength of the Earth's interior; a preliminary result, *Phys. Earth planet. Inter.*, **55**, 234–240.

Kaula, W. M., 1963. Elastic models of the mantle corresponding to variations in the external gravity field, *J. geophys. Res.*, **68**, 4967–4978.

Minster, J. B. & Jordan, H., 1978. Present-day plate motions, *J. geophys. Res.*, **83**, 5331–5354.

Minster, J. B., Jordan, T. H., Molnar, P. & Haines, E., 1974. Numerical modelling of instantaneous plate tectonics, *Geophys. J. R. astr. Soc.*, **36**, 541–576.

Mitrovica, J. X. & Peltier, W. R., 1989. The resolving power of postglacial rebound data, *IASPEI abstracts*, 84.

Montagner, J. P. & Jobert, N., 1981. Investigation of upper mantle structure under young regions of the southeast Pacific using long-period Rayleigh wave, *Phys. Earth planet. Inter.*, **27**, 206–222.

Morelli, A. & Dziewonski, A. M., 1987. Topography of the core–mantle boundary and lateral heterogeneity of the liquid core, *Nature*, **325**, 678–683.

Nakada, M. & Lambeck, K., 1989. Late Pleistocene and Holocene sea-level change in the Australian region and mantle rheology, *Geophys. J.*, **96,** 497–517.

Officer, C. B., Newman W. S., Sullivan, J. M. & Lynch, D. R., 1988. Glacial adjustment and mantle viscosity, *J. geophys. Res.*, **93,** 6397–6409.

Peltier, W. R. & Andrews, J. T., 1976. Glacial isostatic adjustment—1, the forward problem, *Geophys. J. R. astr. Soc.*, **46,** 605–646.

Ricard, Y. & Vigny, C., 1989. Mantle dynamics with induced plate tectonics, *J. geophys. Res.*, **94,** 17 543–17 559.

Ricard, Y. & Sabadini, R., 1990. Rotational instabilities of the Earth induced by dynamically compensated density anomalies in the upper and lower mantle, *Geophys. Res. Lett.*, **17,** 627–630.

Ricard, Y., Fleitout, L. & Froidevaux, C., 1984. Geoid heights and lithospheric stresses for a dynamic Earth, *Annales Geophysicae*, **2,** 267–286.

Ricard, Y., Vigny, C. & Froidevaux, C., 1989. Mantle heterogeneities, geoid and plate motion: a Monte Carlo inversion, *J. geophys. Res.*, **94,** 13 739–13 754.

Richards, M. A. & Hager, B. H., 1984, Geoid anomaly in a dynamic Earth, *J. geophys. Res.*, **89,** 5987–6002.

Richards, M. A. & Hager, B. H., 1988. The Earth's geoid and the large-scale structure of mantle convection, *The Physics of Planets*, pp. 247–272, Wiley, New York.

Richards, M. A. & Hager, B. H., 1989. Effects of lateral variations on long-wavelength geoid anomaly and topography, *J. geophys. Res.*, **94,** 10 299–10 313.

Rubincam, D. P., 1982. Information theory lateral density distribution for Earth inferred from global gravity field, *J. geophys. Res.*, **87,** 5541–5552.

Sabadini, R. & Peltier, W. R., 1981. Pleistocene deglaciation and the Earth's rotation: implications for mantle viscosity, *Geophys. J. R., astr. Soc.*, **66,** 553–578.

Sabadini, R. & Yuen, D. A., 1989. Mantle stratification and long-term polar wander, *Nature*, **339,** 373–375.

Tanimoto, T., 1986. The Backus–Gilbert approach to three-dimensional structure in the upper mantle: II. SH and SV velocity, *Geophys. J. R. astr. Soc.*, **84,** 49–69.

Tarantola, A. & Valette, B., 1982. Generalized non-linear inverse problems solved using the least squares criterion, *Rev. Geophys.*, **20,** 219–232.

Vigny, C., Ricard, Y. & Froidevaux, C., 1991. The driving mechanism of plate tectonics, *Tectonophysics*, in press.

Woodhouse, J. H. & Dziewonski, A. M., 1984. Mapping the upper mantle: three-dimensional modelling of Earth structure by inversion of seismic waveforms, *J. geophys. Res.*, **84,** 5953–5986.

Wu, P. & Peltier, W. R., 1983. Glacial isostatic adjustment and the free air gravity anomaly as a constraint on deep mantle viscosity, *Geophys. J. R. astr. Soc.*, **74,** 377–449.

Yuen, D. A., Sabadini, R., Gasperini, P. & Boschi, E., 1986. On transient rheology and glacial isostasy, *J. geophys. Res.*, **91,** 11 420–11 438.